Rheol Acta (2008) 47:499–508
DOI 10.1007/s00397-007-0238-z

ORIGINAL CONTRIBUTION

Is vorticity-banding due to an elastic instability?

Kyongok Kang · M. Paul Lettinga · Jan K. G. Dhont

Received: 11 May 2007 / Accepted: 19 August 2007 / Published online: 21 February 2008

Abstract A possible mechanism for the vorticity-banding instability is proposed on the basis of experiments with colloidal rod-like particles that exhibit an isotropic–nematic phase transition. The proposed mechanism is similar to the well-known elastic instability for polymer systems that is due to nonuniform elastic deformation of polymer chains as a result of gradients in the local shear rate (the Weissenberg effect). However, the role of polymer chains is now played by inhomogeneities that exist in systems exhibiting vorticity banding. For the rod-like colloidal system investigated here, inhomogeneities are formed during the early stages of phase separation. Nonuniform deformation of these inhomogeneities are thus proposed to lead to hoop stresses which give rise to banded structures where there is secondary, weakly rolling flow within each of the bands. Many of the features found experimentally for the rod-like colloidal system can be understood on the basis of this proposed mechanism. For different types of systems that also show vorticity banding, inhomogeneities can be identified, which might lead to vorticity banding for the same reasons as for the rod-like colloidal systems studied here.

Keywords Instability · Dispersions · Phase separation

Paper presented at 4th Annual European Rheology Conference, AERC, April 12–14, Napels, Italy.

K. Kang (✉) · M. P. Lettinga · J. K. G. Dhont
Institute für Festkörper Forschung (IFF), Weiche Materie,
Forschungszentrum Jülich,
52425 Jülich, Germany
e-mail: k.kang@fz-juelich.de

Introduction

Two types of banding transitions have been found experimentally in various types of complex solutions, which are referred to as gradient banding and vorticity banding. In case of gradient banding, typically two regions with different shear rates coexist in the stationary state, where in each of the two regions the shear rates are essentially constant, independent of position (see, for example, Berret 1997; Olmsted et al. 2000). The gradient-banding instability occurs when the shear stress (the flow-gradient component of the stress tensor) of the homogeneously sheared system decreases with increasing shear rate. The molecular origin of the accompanied severe shear-thinning behavior is relatively well understood. The origin of the vorticity-banding instability, however, is not yet understood. In the present paper, we propose a possible mechanism for this instability that is related to hoop-stresses generated by nonuniform shear-induced stretching of inhomogeneities. These inhomogeneities can be due to early stage phase separation; they can be self-assembled structures like in worm-like micellar, or they can be aggregates in weakly flocculating colloids. The nonuniform deformation of such inhomogeneities gives rise to elastic normal forces which set the fluid in weakly rolling motion. The rolls correspond to the observed bands that are stacked in the vorticity direction. The mechanism underlying the vorticity-banding instability is thus analogous to the well-known elastic instability of polymer systems, leading to the Weissenberg effect (see Weissenberg 1947), where the role of polymer chains is now played by the inhomogeneities.

Experiments on fd-virus suspensions will be discussed, where vorticity banding is found within the isotropic–nematic two-phase region, which partly extend on earlier work by Kang et al. (2006). Fd virus is a stiff, long, and thin colloidal rod, suspensions of which are model systems

for monodisperse rods. Inhomogeneities are, in this case, due to early stage isotropic–nematic phase separation. The experimental findings discussed in the present paper that can be understood on the basis of the proposed mechanism mentioned above include (1) the different vorticity-banding kinetics depending on whether phase separation leads to bi-continuous structures or isolated inhomogeneities just before banding occurs, (2) the finite shear-rate range where vorticity banding is found, (3) the couette-cell gap-width dependence of the shear-rate region where banding occurs, (4) the gap-width dependence of the final vorticity-band width, and (5) the observed rolling flow within the bands.

This paper is organized as follows. In Section Experiments with fd-virus suspensions, we discuss experimental results on fd-virus suspensions, some of which are also discussed by Kang et al. (2006). The mechanism leading to vorticity banding, as mentioned above, will be discussed in Section A possible mechanism for vorticity banding. Experimental findings will be interpreted on the basis of the proposed mechanism in Section Intuitive explanation of vorticity-banding characteristics of fd-virus suspensions and of other systems, where other vorticity-banding systems are also discussed within the scope of the proposed mechanism.

Experiments with fd-virus suspensions

Fd virus is a stiff, rod-like virus of colloidal dimensions, with a thickness of D=6.6 nm, a length of L=880 nm, and a persistence length of 2,200 nm. We used suspensions with a high ionic strength (20 mM TRIS buffer, pH=8.15 with 100 mM added NaCl) where dextran is added (radius of gyration 16 nm) to enhance isotropic–nematic phase separation and vorticity-band formation. Samples were prepared as follows. First, we prepare a homogeneous solution of fd virus at an overall concentration of 22.1 mg/ml and the appropriate dextran concentration. This mixture is then left to phase separate under gentle centrifugation for about 24 h, to establish separation into two bulk phases. Then a volume V_{nem} from the lower, nematic bulk phase and a volume V_{iso} from the upper, isotropic bulk phase are mixed. This is the mixture that is used in our shear experiments. This procedure of sample preparation ensures that the chemical potential of dextran is independent of the total fd-virus concentration. Experiments are performed for two rod concentrations Φ_{nem}= 0.23 and 0.35, where $\Phi_{\mathrm{nem}}=V_{\mathrm{nem}}/(V_{\mathrm{nem}}+V_{\mathrm{iso}})$. Unless stated otherwise, the dextran concentration in the inhomogeneous suspension is 10.6 mg/ml.

Shear experiments are done in an optical couette cell with a stationary outer cylinder and a rotating inner cylinder. The gap width of the couette cell can be varied from 1.0 to 2.5 mm. The sample is pre-sheared at a shear rate of 10 s^{-1} for at least 10 min. This shear rate is far above the highest shear rate that bounds the two-phase region. Experiments are done by quenching from this high shear rate to a lower shear rate where vorticity banding occurs. Vorticity banding of fd-virus suspensions is observed both under controlled shear rate and controlled shear stress conditions, within a limited part of the two-phase paranematic–nematic region as bounded by the isotropic–nematic binodal in the shear-rate vs fd-concentration plane (see also Kang et al. 2006). For a fixed fd-concentration, banding occurs within a shear-rate interval $\left(\dot{\gamma}_+,\dot{\gamma}_+\right)$, where the "border shear rates" $\dot{\gamma}_-$ and $\dot{\gamma}_+$ lie within the two-phase region.

Vorticity bands are visualized by placing the couette cell between polarizers that are slightly off from a crossed alignment of polarizations. Time resolved transmitted intensity profiles are recorded with a CCD camera equipped with a telecentric lens. An example of such intensity profiles is given in Fig. 1. The two types of bands appear as alternating dark and bright regions. Average band widths are obtained through a Fourier mode analysis of the resulting transmitted intensity profiles, where the height of bright and dark bands is equal. Details are given by Kang et al. (2006).

The banded patterns that are discussed here are similar to that found for the well-known Taylor instability. The Taylor instability for the fd-virus suspensions has been observed to occur at a shear rate typically equal to about 25 s^{-1}. This shear rate is about a factor of 50–100 larger than the typical shear rates where vorticity banding is seen. We are thus far below the critical shear rates at which the Taylor-banding instability occurs.

Outside the banding region, the suspension merely phase separates into a sheared bulk isotropic state (the "paranematic phase") and a sheared bulk nematic phase, without the occurrence of a banded structure. Confocal images of morphologies of phase separating fd-virus suspensions at various concentrations after a shear-rate quench from 10 s^{-1} to a zero shear rate are shown in Fig. 2. These images are taken 10 min after the shear quench. The bright regions are nematic regions, the dark regions are isotropic. On increasing the rod concentration, the difference in rate of decomposition leads to isolated inhomogeneities at high rod concentrations and a bi-continuous structure at low concentrations at the instant where banding sets in. The observed spinodal decomposition at low concentration and nucleation and growth at higher concentration indicates that the initial state, before demixing occurred, is aligned due to the high shear rate before the shear-rate quench. Demixing kinetics of fd-virus suspensions is studied in detail by Lettinga et al. (2005).

Vorticity banding is only found within the isotropic–nematic two-phase region, which indicates that the inhomogeneities that are formed after the quench are essential for the banding instability. Without these inhomogeneities,

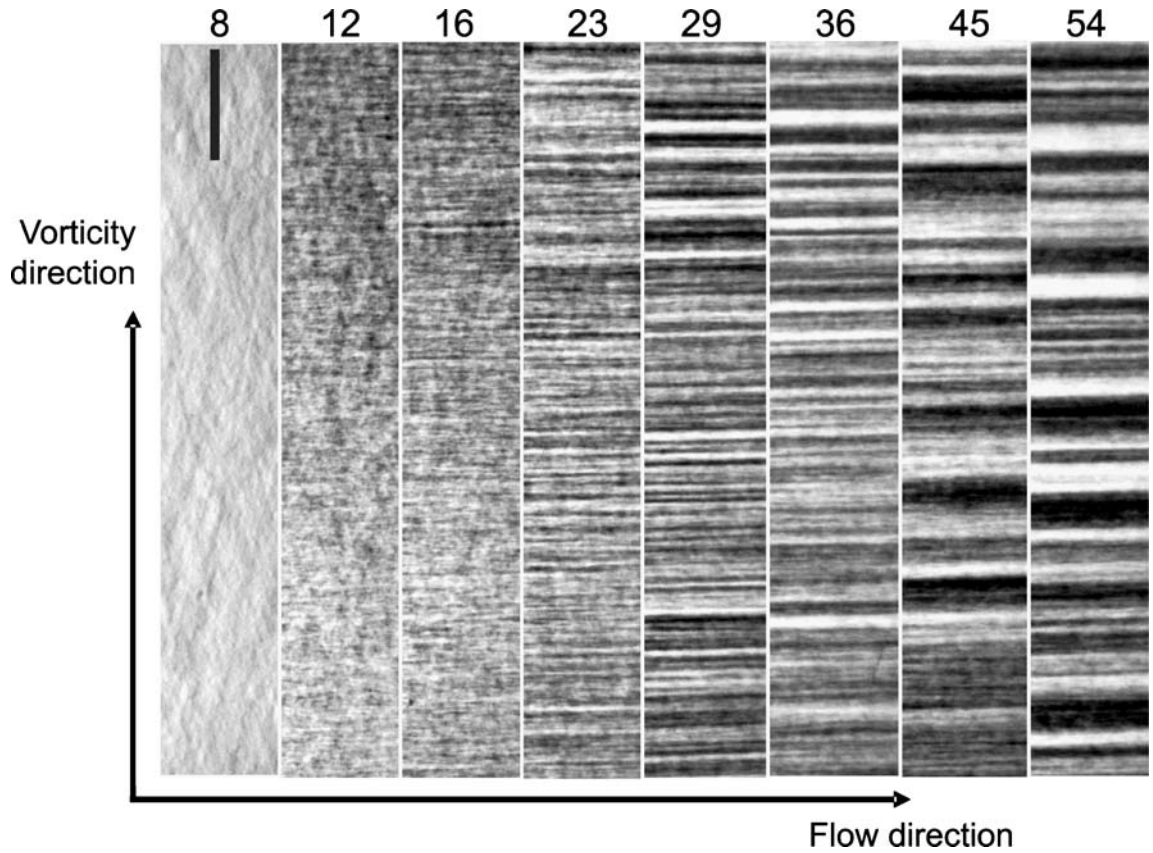

Fig. 1 An example of intensity profiles at different times. The numbers are times in minutes after the shear-rate quench. The *bright and dark bands* are the two types of vorticity bands that are formed. The *left upper bar* is 1 mm long. Banding sets in 10 min after the quench. The *most left figure* taken 8 min after the quench thus shows shear-stretched inhomogeneities, before banding occurred

vorticity banding does not occur. It is therefore to be expected that the kinetics of vorticity-band formation depends on the fd concentration, as according to Fig. 2, the morphology of inhomogeneities that is formed during the initial stages of demixing varies with the fd concentration. This is indeed the case as can be seen from Fig. 3, where the band width as a function of time right after the shear quench is plotted. Right after the quench, inhomogeneities are shear-stretched, giving rise to a decrease of the apparent "band width". At a well-defined time, vorticity banding sets in, and the band width increases with time. The two plots (a) and (b) on the left are for 23% and the two plots (c) and (d) on the right are for 35%. The time where banding sets in is 10 min for 23% and 15 min for 35%. For the two upper plots (a) and (c), the shear rate is close to the lower border shear rate. The two lower figures,

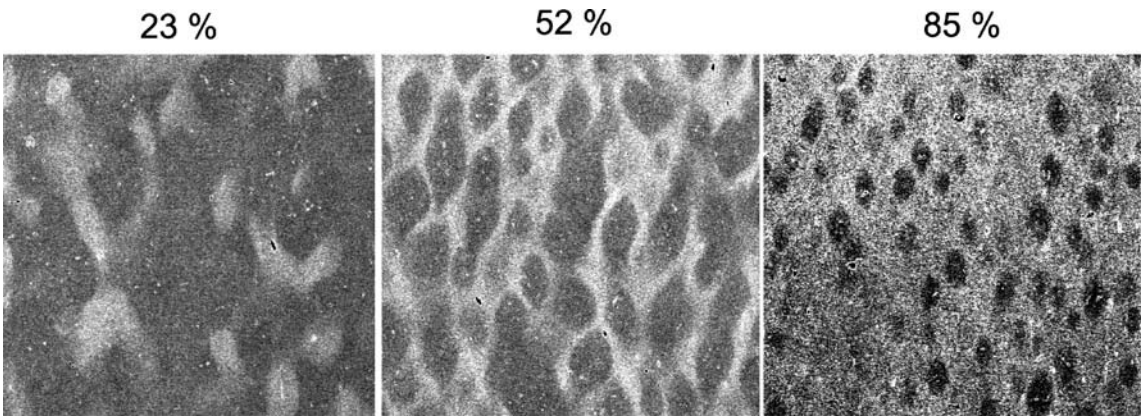

Fig. 2 Confocal images of fd-suspensions with increasing Φ_{nem} (*from left to right*, as indicated in the figure), after a quench from shear rate 10 s^{-1} to a zero shear rate, taken 10 min after the shear quench. The spinodal is located at approximately 52% (Lettinga et al. 2005)

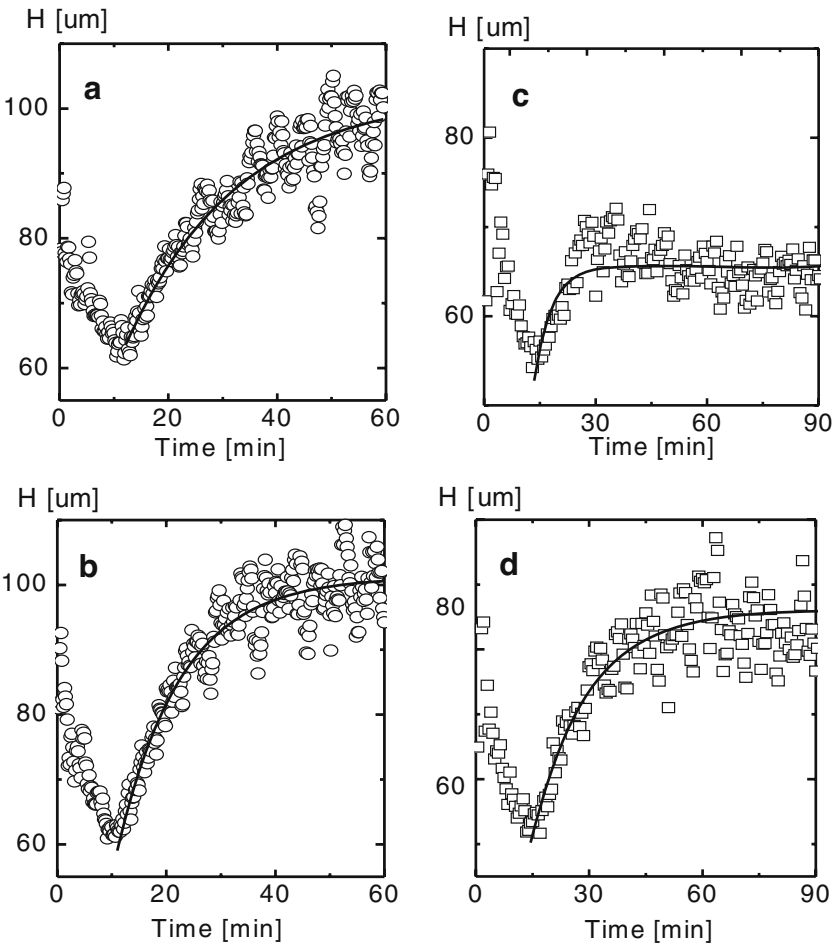

Fig. 3 The time dependence of the band width for two different fd-rod concentrations: **a** and **b** for Φ_{nem}=0.23%, and **c** and **d** for 0.35%. **a** $\dot{\gamma}$=0.17 s^{-1} close to the lower border shear rate and **b** $\dot{\gamma}$=0.29 s^{-1} in the middle of the banding region for 23%, and similarly **c** $\dot{\gamma}$=0.29 s^{-1} and **d** $\dot{\gamma}$=0.40 s^{-1} for 35%

(b) and (d) are for a shear rate in the middle of the shear-rate interval $\left(\dot{\gamma}_{-},\dot{\gamma}_{+}\right)$ where vorticity banding occurs. The solid curves are a fit to a single time exponential. For the lower concentration of 23%, close to the lower border shear rate $\dot{\gamma}_{-}$ (see Fig. 3a), the growth time is much larger than for the shear rate in the middle of the banding interval (see Fig. 3b). The total increase of the band width, however, is approximately the same for both cases (~40 μm). On the contrary, for the higher concentration of 35%, the growth time is approximately the same for the two shear rates, but the total increase of the band width is much smaller at the lower-border shear rate (see Fig. 3c and d). Hence, vorticity banding ceases to occur due to the divergence of the growth time in the case of a bi-continuous, spinodal-like structure, and banding ceases to occur due to a vanishing amplitude in the case of isolated inhomogeneities. Interestingly, the shear-rate interval $\left(\dot{\gamma}_{-},\dot{\gamma}_{+}\right)$ where vorticity banding occurs depends on the gap width of the shear cell, as can be seen from Fig. 4. For the lower fd concentration with Φ_{nem}=0.23, where we have a bi-continuous structure, the shear-rate region where banding occurs widens with increasing gap width. For the higher fd concentration, however, where isolated inhomogeneities are formed, both border shear rates decrease with increasing gap width. The shear rate interval where banding occurs now decreases with increasing gap width. As will be discussed in Section Intuitive explanation of vorticity-banding characteristics of fd-virus suspensions and of other systems, the gap-width dependence of both $\dot{\gamma}_{-}$ and $\dot{\gamma}_{+}$ is probably due to the change of gradients in local shear rates. The different behavior for the two concentrations is due to differences of the elastic properties of the inhomogeneities formed during the initial stages of demixing for Φ_{nem}=0.23 and 0.35. As can be seen from Fig. 4c, the band width in the stationary state depends on the gap width. Vorticity bands become broader on increasing the gap width of the shear cell.

To investigate whether the shear rate is constant throughout the vorticity bands or whether they exhibit internal rolling flow, we tracked the position of a tracer sphere along the vorticity direction. This experiment is performed on a sample with a relatively high dextran concentration (12.3 mg/ml) and a relatively low fd concentration (Φ_{nem}=0.17) leading to more pronounced bands with a typical band width of about 1 mm. The cell gap width in this experiment is 1.5 mm, and the shear rate is 0.88 s^{-1}. As can be seen in Fig. 5, there is an oscillatory

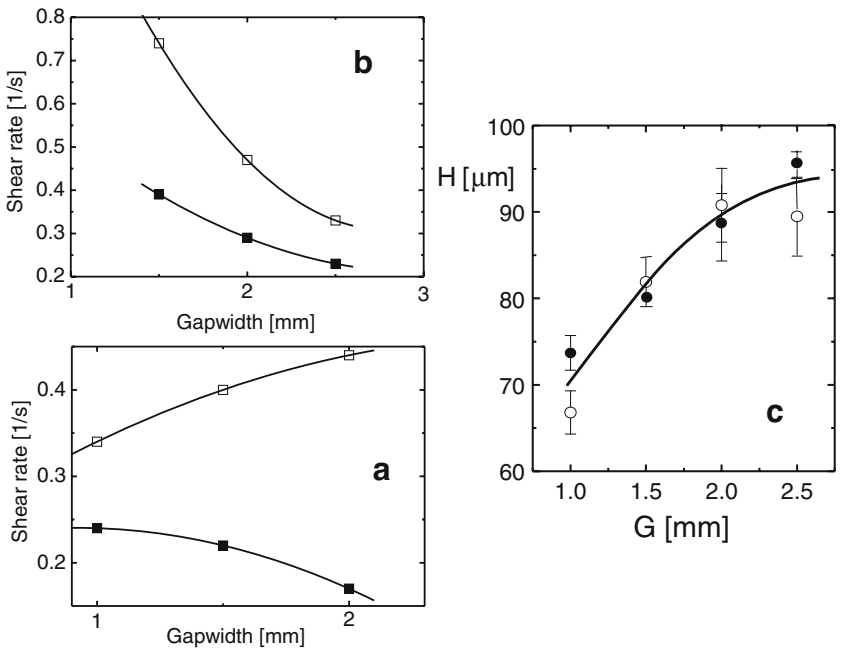

Fig. 4 The variation of the upper-border shear rates (*empty squares*) and lower-border shear rates (*filled squares*) with the cell gap width for the two concentrations Φ_{nem}=23% (**a**) and 35% (**b**). **c** The band width in the quasi stationary state as a function of the couette cell gap width. The data points are for 23% at shear rates 0.29 s^{-1} (*empty circles*) and 0.34 s^{-1} (*filled circles*)

motion of the tracer sphere along the vorticity direction, indicating that the bands are in (weakly) internal rolling flow. There is also a drift downwards as a result of sedimentation. No oscillations of the shear stress under controlled shear-rate conditions have been observed in the stationary vorticity-banded state. In Section A possible mechanism for voricity banding, we will discuss a possible mechanism leading to rolling flow. Furthermore, the rod concentration is the same within the two bands, as can be seen from the fluorescent image in the right panel in Fig. 6, where the fd rods are fluorescently labeled. The left panel shows the banded structure as visualized through birefringence. The right figure probes the same area, and shows the fluorescent intensity from a laser beam directed along the vorticity direction. As can be seen, the fluorescent intensity is homogeneous along the vorticity direction, implying that the concentrations within the bands are similar. Within experimental noise (about 2%), no contrast between bands could be seen.

A possible mechanism for vorticity banding

A recently proposed mechanism by Fielding (2007) for vorticity banding involves the formation of a gradient banded flow, before vorticity banding occurs. The gradient-banded interface generates normal body forces that set the suspension in motion along the gradient direction. This would ultimately lead to vorticity banding where the bands are in internal rolling flow. Kang et al. (2006) report on stress measurements for fd-virus suspensions just before vorticity banding occurs. The shear stress is found to be a monotonically increasing function of shear rate. Furthermore, no decrease of the measured shear stress is observed during banding (experiments like in Fig. 1 given by Lettinga and Dhont 2004 have been extended to a much larger time range). We neither found a van der Waals loop-like behavior of the stress nor observed a stress plateau. There is thus no sign that gradient banding plays a role in the formation of vorticity bands in the fd-virus suspensions.

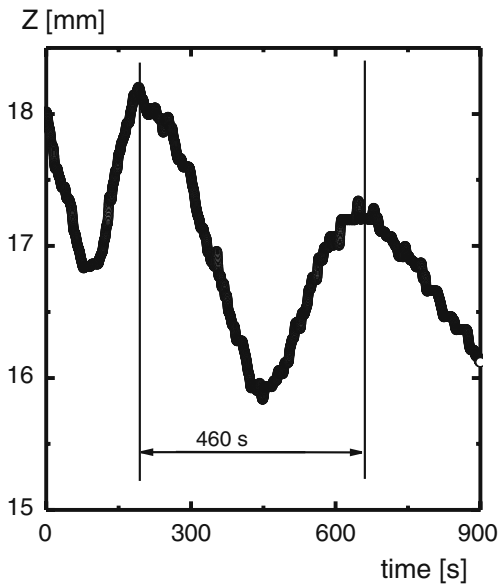

Fig. 5 The position of a tracer sphere (diameter 50 μm) in the vorticity direction within a band as a function of time. The dextran concentration was 12.3 mg/ml, the cell gap width is 1.5 mm and Φ_{nem}=0.15

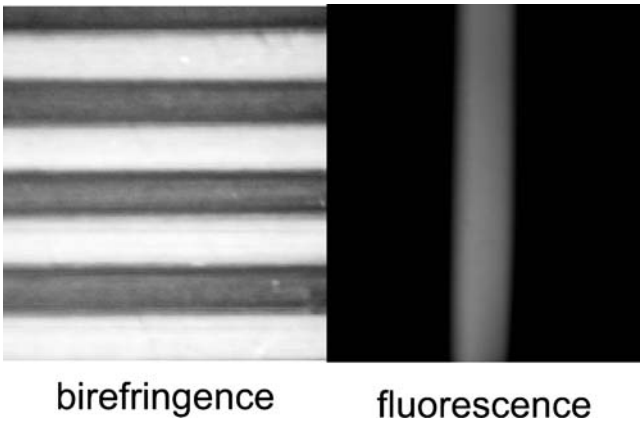

Fig. 6 *Left figure*: the banded structure. The dextran concentration here is 12.3 mg/ml. *Right figure:* the same are as in the left figure, where now the fluorescent intensity of a laser beam along the vorticity direction is probed. Here, the fd virus is fluorescently labeled

This suggests that a different mechanism is probably involved for vorticity banding of fd-virus suspensions. Schmitt et al. (1995) proposed a mechanism for the development of a banded structure along the vorticity direction that involves spinodal decomposition, where the mass diffusion coefficient is negative. For our fd-virus suspensions, however, banding is found throughout the two-phase region, including the meta-stable region where the mass diffusion coefficient (and also the orientational diffusion coefficient) is positive. This indicates that the proposed mechanism by Schmitt et al. (1995) does not apply to our system of rod-like colloids. The rolling flow within the bands and the monotonically increasing shear stress with increasing shear rate show that the stationary state is not a state where the shear rate is constant throughout the gap, as was assumed in earlier theories by Olmsted and Lu (1999), Olmsted (1999), Goveas and Olmsted (2001), and Aradian and Cates (2006).

In view of the experimental results presented in the previous section, we propose a mechanism that is similar to the elastic instability for polymer systems, known as the Weissenberg effect. The Weissenberg effect is due to normal stresses in the gradient direction, so-called hoop stresses, which are generated by nonuniform elastic deformation of polymer chains (see, for example, Weissenberg 1947; Larson et al. 1990; Pakdel and McKinley 1996, and Groisman and Steinberg 1998). This elastic instability has the following microscopic origin. In a couette geometry, the local shear rate increases slightly towards the inner cylinder. This leads to a more pronounced stretching of the part of a polymer chain that is closer to the inner cylinder and to a less pronounced stretching of the part of a polymer chain further away from the inner cylinder (see Fig. 7a). On average, this nonuniform stretching leads to a body force that is directed towards the inner cylinder. When these normal forces are large enough, this leads to a flow towards the inner cylinder. We note that volume elements do not immediately move towards the inner cylinder once the instability occurs. The flow towards the inner cylinder is initiated in the bulk of the suspension and is accompanied by a back flow (see the stability analysis later in this section). In the resulting stationary state, this leads to bands assembled along the vorticity direction, where there is a secondary, rolling flow within the bands. Near the surface of the polymer system, the upwards flow along the inner cylinder leads to the well- known "rod-climbing" effect. The vorticity-banding instability is proposed to be of the same origin, where the role of polymer chains is now played by inhomogeneities (see Fig. 7b). In the case of the fd-virus suspensions discussed above, the inhomogeneities formed during the initial stages of phase separation are nonuniformly deformed, leading to hoop stresses which give rise to banding.

The proposed mechanism that underlies the vorticity instability can be specified in somewhat more detail by means of a stability analysis. The crude stability analysis described below explains the major features of the vorticity instability. For sufficiently shallow inhomogeneities, the internal structure of the inhomogeneities will be able to adjust to the imposed flow such that the body force B_y in the y direction (the gradient direction) is zero. When inhomogeneities become more pronounced, however, such an adjustment may not be possible anymore, resulting in a nonzero body force, which leads to flow along the gradient direction. We ask for the amplitude of inhomogeneities under which a change in the amplitude of the inhomogeneities leads to flow in the gradient direction of the initial flow profile. Within the "Weissenberg scenario for vorticity banding", a nonzero flow velocity u_y along the y- direction

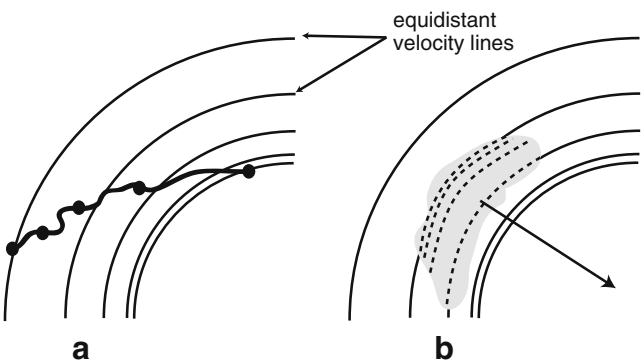

Fig. 7 **a** A schematic of the origin of the Weissenberg effect, where polymer chains are nonuniformly stretched, as indicated by the dots, which would be equidistant for uniform stretching. **b** Nonuniform deformation of an inhomogeneity. The *dotted lines* indicate the nonuniform deformation, like the dots for the polymer chain. The lines are equidistant flow velocity lines. The *arrow* represents the normal force towards the inner cylinder

initiates vorticity banding. As the discrete nature of the inhomogeneities along the flow direction is relatively unimportant, the gradient component of the Navier–Stokes equation reads,

$$\rho_m\left[\frac{\partial}{\partial t}+u_y\frac{\partial}{\partial y}+u_z\frac{\partial}{\partial z}\right]u_y(y,z,t)=B_y(y,z,t), \tag{1}$$

where u_z is the flow velocity in the z direction (the vorticity direction). Let δu_y be the small change of u_y due to a change of the amplitude of inhomogeneities, and δB_y the accompanied change of the body force. As $u_z=0$ before banding occurs, linearization of the Navier–Stokes Eq. 1 gives,

$$\rho_m\frac{\partial\delta u_y(y,z,t)}{\partial t}=\delta B_y(y,z,t). \tag{2}$$

The z dependence of both δu_y and δB_y is approximately sinusoidally $\sim\exp\{ikz\}$, where $\Lambda=2\pi/k$ is the typical distance between inhomogeneities (as sketched in Fig. 8a). This wavelength corresponds to the most pronounced Fourier mode of the intensity profile taken at 12 min as given in Fig. 1. The y dependence of δB_y is much more complicated and is related to the nonlinear deformation of the inhomogeneities along the gradient direction. Substitution of the forms,

$$\begin{aligned}\delta u_y(y,z,t)&=\delta\bar{u}_y(y)\ \exp\{ikz-\Gamma t\},\\ \delta B_y(y,z,t)&=\delta\bar{B}_y(y)\ \exp\{ikz-\Gamma t\}.\end{aligned} \tag{3}$$

into Eq. 3 leads to,

$$-\rho_m\Gamma\delta\bar{u}_y(y)=\delta\bar{B}_y(y). \tag{4}$$

Here, $\Gamma>0$ is the flow relaxation time in case no vorticity banding occurs, while $\Gamma<0$ when the system is unstable against vorticity banding. A theoretical prediction for the behavior of the body force B_y for rod-like colloids can be based on the equations of motion for the density and order parameter, and the constitutive equation for inhomogeneous suspensions as derived by Dhont and Briels (2002, 2003). Here, the body force is expressed in terms of integrals over the probability density $\rho(r,\hat{u},t)$ for the position $\mathbf{r}$ of a rod and its orientation specified by the unit vector $\hat{u}$. The constitutive equation derived by Dhont and Briels (2003) contains three distinct contributions: there is a Brownian body force, a contribution due to rod–rod interactions and a contribution due to direct coupling of flow to microstructural order. The Brownian body force and the coupling contribution are linear in the probability density, while the interaction contributions to the body force are bilinear. The probability density is now written as $\rho(\mathbf{r},\hat{u},t)=A\hat{\rho}_0(\mathbf{r},\hat{u})+\delta A\hat{\rho}_1(\mathbf{r},\hat{u},t)$, where $\hat{\rho}_0$ and $\hat{\rho}_1$ are re-normalized densities, where their prefactors A and δA specify their amplitude. The density $\hat{\rho}_0$ is supposed to lead to a zero body force in the gradient direction. We are looking for those amplitudes A, above which the probability density is not able anymore to adjust itself to the imposed flow profile such that the body force remains zero. Upon linearization of the above mentioned contributions to the body force with respect to δA, the following possible contributions to δB_y result. The linear terms in the density give rise to contributions that do not involve the amplitude A. Normal body forces vary like $\sim(\dot{\gamma}\tau)^2$ for small shear rates, where τ is the relaxation time of shear-induced deformations of inhomogeneities. For high shear rates, normal forces shear-thin to a relatively small value. Hence, the linear terms in density give rise to contributions of the form $\sim(\dot{\gamma}\tau)^2 f(\dot{\gamma}\tau)\delta A$, where f tends to a nonzero constant for small shear rates and tends essentially to zero for high shear rates. For convenience, we shall use the simplest function with these limiting properties: $f(\dot{\gamma}\tau)=1\Big/\left[1+(\dot{\gamma}\tau)^4\right]$. The rod–rod interaction contributions to the body force which are bilinear in the density similarly lead to contributions of the form $\sim(\dot{\gamma}\tau)^4$

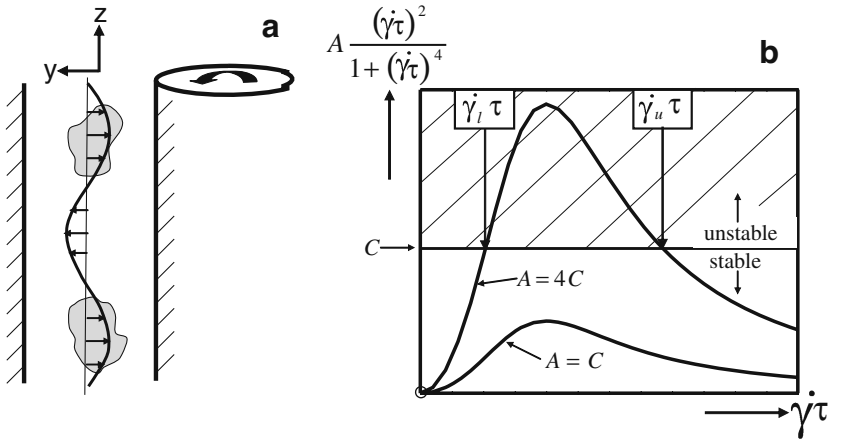

Fig. 8 **a** The flow field along the gradient direction in the initial stage of vorticity banding. The *light grey inclusions* represent inhomogeneities. **b** Stability diagram for vorticity banding within the "Weissenberg scenario". A measures the magnitude of inhomogeneities. For the lower curve, $A=C$, while for the upper curve, $A=4C$. The system is unstable in the shear-rate interval $(\dot{\gamma}_l,\dot{\gamma}_u)$, where $\dot{\gamma}_l$ is "the lower border shear rate" and $\dot{\gamma}_u$ is the "upper border shear rate"

$f^2\left(\dot{\gamma}\tau\right)A\delta A$, as $\hat{\rho}_0$ and $\hat{\rho}_1$ are essentially equal. The linear change of the body force due to a slight change of the density is thus of the form,

$$\delta \bar{B}_y = \left\{ C_1 + C_2 A \frac{\left(\dot{\gamma}\tau\right)^2}{1+\left(\dot{\gamma}\tau\right)^4} \right\} \frac{\left(\dot{\gamma}\tau\right)^2}{1+\left(\dot{\gamma}\tau\right)^4} \delta A, \qquad (5)$$

where the constant C_1 is linear in $\hat{\rho}_1$ and C_2 is bilinear in $\hat{\rho}_0$ and $\hat{\rho}_1$. These constants are determined by the internal structural properties of the inhomogeneities. Without loss of generality, A and δA can be taken positive. Suppose that δu_y is negative, implying that the flow is directed towards the inner cylinder at positions where inhomogeneities are present and a "backflow" occurs in between the inhomogeneities, as sketched in Fig. 8a (the analysis given below proceeds similarly when δu_y is negative). From Eqs. 4 and 5, the following instability criterion for which $\Gamma<0$ is then found,

$$C_1 + C_2 A \frac{\left(\dot{\gamma}\tau\right)^2}{1+\left(\dot{\gamma}\tau\right)^4} < 0. \qquad (6)$$

As no banding is expected when interactions are absent (in which case $C_2=0$), the constant C_1 must be positive. Banding can thus occur when $C_2<0$. The instability condition can thus be rewritten as,

$$A \frac{\left(\dot{\gamma}\tau\right)^2}{1+\left(\dot{\gamma}\tau\right)^4} > C, \qquad (7)$$

where $C = -C_1/C_2 > 0$. The corresponding stability diagram is given in Fig. 8b. The form $\left(\dot{\gamma}\tau\right)^2 \Big/ \left[1+\left(\dot{\gamma}\tau\right)^4\right]$ has a single maximum at $\dot{\gamma}\tau = 1$, with a maximum value of 1/2. Hence, when $A<2C$, there is no instability (see the lower curve in Fig. 8b, for which $A=C$). In this case, inhomogeneities are not sufficiently pronounced to produce body forces which lead to flow along the gradient direction. That a minimum strength of inhomogeneities is required for vorticity banding is evidenced by the fact that banding occurs only at a characteristic time after the shear-rate quench, where phase separation led to sufficient inhomogeneities (see Fig. 3). When $A>2C$, an instability occurs only in a limited shear-rate range $\left(\dot{\gamma}_l, \dot{\gamma}_u\right)$, with $\dot{\gamma}_l > 0$ (as indicated in the upper curve in Fig. 8b, for which $A=4C$). This is also seen in our experiments, where for a given fd concentration, banding indeed occurs in a shear-rate range where the lower border shear rate is nonzero. A threshold shear rate is needed to produce body forces along the gradient direction, while shear thinning of normal stresses leads to zero body forces, rendering the system stable again at higher shear rates. A more precise analysis can be performed using the constitutive relation as derived by Dhont and Briels (2002, 2003).

To further validate the proposed mechanism, the gap width dependence of the shear rate for the onset of elastic instability, as given in Fig. 4a and b, could be compared to theory. Larson et al. (1990) predicts a $G^{1/2}$-dependence on the gap width G. However, there are too few data points in Fig. 4a and b to confirm this prediction. It is also not possible to estimate the critical Weissenberg number where banding first occurs, as this involves the relaxation time of the nonuniformly stretched inhomogeneities to their homogeneous state. It is not clear how to measure or estimate such a relaxation time.

The volume fraction of dextran is about 0.15, and therefore below the overlap concentration. The dextran is therefore dilute and far from being entangled. Dextran as such is therefore not at the origin of the observed banding. In fact, for a given dextran concentration, vorticity banding ceases to occur outside the paranematic–nematic two-phase region. The role of dextran is to induce depletion attractions between the rods, which apparently has an appreciable effect on the mechanical properties of the inhomogeneities.

Intuitive explanation of vorticity-banding characteristics of fd-virus suspensions and of other systems

Assuming that the mechanism described in the previous section is at the origin of vorticity banding, a number of the experimental findings for the fd-virus suspensions can be understood intuitively.

Based on the proposed mechanism, it is immediately clear why banding is observed only within the two-phase region. Without the presence of elastically deformable inhomogeneities that are formed due to phase separation, hoop stresses cannot be generated, and banding will not occur.

Banding is observed only within a limited shear-rate region $\left(\dot{\gamma}_-, \dot{\gamma}_+\right)$, with $\dot{\gamma}_- > 0$. The overall shear rate must exceed a minimum value to lead to normal stresses that are sufficiently large to lead to rolling flow. Banding probably ceases to occur at higher shear rates because the extent of inhomogeneities in the gradient direction becomes too small to achieve sufficient nonuniform deformation in that direction.

For a couette geometry, local gradients in shear rate increase with increasing gap width. Such larger gradients in shear rate lead to stronger nonuniform stretching and therefore to larger hoop stresses. This explains why $\dot{\gamma}_-$ decreases with increasing gap width (see Fig. 4a and b). That the upper border shear rate $\dot{\gamma}_+$ decreases for increasing gap width in case of isolated inhomogeneities and increases

in case of a bi-continuous structure is unclear. It reflects the different elasticity of inhomogeneities in a bi-continuous, spinodal-like structure or isolated inhomogeneities. The stronger hoop stresses for larger gap widths evidently leads to larger band widths, which is indeed observed (see Fig. 4c).

Vorticity banding is found, independent of whether the shear rate or shear stress is controlled. This agrees with the proposed mechanism, as normal stresses are important, independent of whether shear rate or shear stress is controlled during the experiment.

Finally, the same observed rolling flow within the bands for the polymer systems is expected, as the same mechanism is responsible for the observed banding.

Vorticity banding is observed in different kinds of systems. Inhomogeneities can be identified in all these systems that might be elastically nonuniformly deformed, leading to banding as proposed above. Vorticity banding has been seen in nanotube suspensions by Lin-Gibson et al. (2004), which are partly aggregated. These aggregates are the necessary inhomogeneities to induce the hoop stresses leading to banding. The normal stress measurements by Lin-Gibson et al. (2004) indeed indicate that such stresses play a role in vorticity banding for these systems. Similar aggregates of weakly flocculating spherical colloidal particles are reported by Vermant et al. (1999) to give rise to vorticity banding. Stationary vorticity banding has also been observed by Bonn et al. (1998) for worm-like micellar systems. Either the worm-like micelles serve here as the inhomogeneities or a shear-induced nematic phase is formed, leading to the same kind of inhomogeneities for our fd-virus suspension.

Vorticity banding is occasionally connected to a strong shear thickening (like for the worm- like micelles found by Bonn et al. 1998), where the shear stress exhibits a discontinuity, as schematically depicted in Fig. 9. Assuming that the shear rate is spatially constant and equal to the applied shear rate throughout the system, the accompanied multi-valued form of the flow curve is a necessary condition for the existence of vorticity bands. The two shear stresses indicated in Fig. 9 correspond, in that case, to the stresses carried by the two different microstructures (or phases) that exist within the bands. However, such a shear-thickening behavior is not observed in our fd-virus suspensions. What might happen for systems that exhibit such a shear thickening is that inhomogeneities exist due to a shear-induced phase transition of a phase with a much higher shear viscosity compared to structure at low shear-rates. Highly viscous inhomogeneities could be formed during the initial stages of this shear-induced phase transition, which then lead to vorticity banding according to the proposed mechanism in the previous section (personal communication with John R. Melrose).

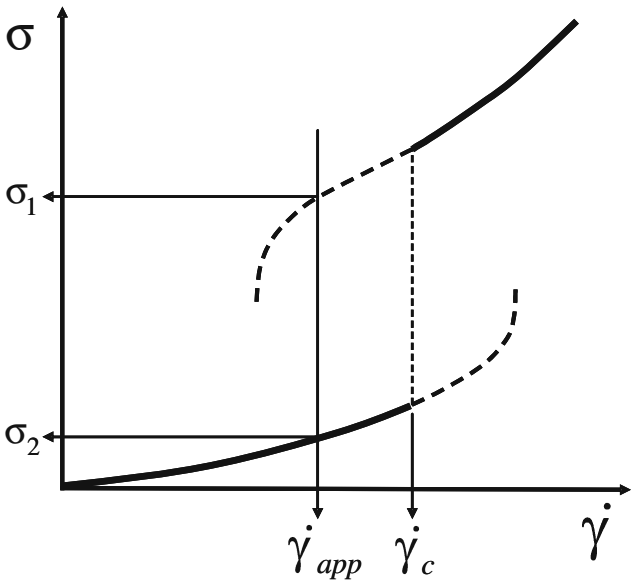

Fig. 9 The shear viscosity as a function of shear rate, where beyond a critical shear rate $\dot{\gamma}_c$, a shear-induced, very viscous phase is formed. The *two dashed branches* are (meta-table) states. In case the shear rate is equal to the applied shear rate $\dot{\gamma}_{app}$ throughout the gap, the two types of vorticity bands support the stresses σ_1 and σ_2

Summary

Experiments on vorticity banding of suspensions of colloidal rod-like particles (fd virus) reveal the importance of inhomogeneities that are formed during the initial stages of isotropic–nematic phase separation. Vorticity banding occurs only within the two-phase region and banding kinetics depends on whether the inhomogeneities are formed due to spinodal decomposition or a mix of spinodal decomposition and nucleation and growth. Furthermore, the shear-rate region where banding occurs and the final band width depend on the gap width of the couette cell, and there is a secondary weakly rolling flow within the bands. This lead us to propose a mechanism that gives rise to the vorticity-banding instability, which is similar to the well-known elastic instability of polymer systems (the Weissenberg effect). Instead of nonuniform deformation of polymer chains that lead to hoop stresses giving rise to band formation, the inhomogeneities are nonuniformly deformed in case of vorticity banding. The vorticity-banding instability is thus proposed to be similar to the Weissenberg effect, where the role of polymer chains is now played by inhomogeneities. Many of the observed banding characteristics can be understood intuitively on the basis of this mechanism.

Inhomogeneities can be identified in other systems that exhibit vorticity banding. It remains, however, to be further investigated whether these other systems also exhibit banding due to the proposed elastic instability. The main

features that should be investigated are whether there is a secondary, rolling flow within the bands and whether the banding characteristics depend on the properties of the inhomogeneities that are present. A quantitative understanding requires a theory that includes stresses generated by nonuniformly stretched inhomogeneities.

It would be interesting to perform normal stress measurements in a cone-plate geometry. However, in view of the very long oscillation time of the rolling flow, the normal stress differences for the fd-virus suspensions might be too small to measure with the present available rheometers.

References

Aradian A, Cates ME (2006) Phys Rev E 73:041508
Berret J-F (1997) Langmuir 13:2227
Bonn D, Meunier J, Greffier O, Al-Kahwaji A, Kellay H (1998) Phys Rev E 58:2115
Dhont JKG, Briels WJ (2002) J Chem Phys 117:3992
Dhont JKG, Briels WJ (2003) J Chem Phys 118:1466
Fielding SM (2007) Phys Rev E 76:016311
Goveas JL, Olmsted PD (2001) Eur Phys J E 6:79
Groisman A, Steinberg V (1998) Phys Fluids 10:2451
Kang K, Lettinga MP, Dogic Z, Dhont JKG (2006) Phys Rev E 74:026307
Larson RG, Shaqfeh ESG, Muller SJ (1990) 218:573
Lettinga MP, Dhont JKG (2004) J Phys Cond Mat 38:S3929
Lettinga MP, Kang K, Imhof A, Derks D, Dhont JKG (2005) J Phys Cond Mat 17:3609
Lin-Gibson S, Pathak JA, Grulke EA, Wang H, Hobbie EK (2004) Pys Rev Lett 92:048302
Olmsted PD, Lu C-Y (1999) Phys Rev E 60:4397
Olmsted PD (1999) Europhys Lett 48:339
Olmsted PD, Radulescu O, Lu C-Y (2000) J Rheol 44:257
Pakdel P, McKinley GH (1996) Phys Rev Lett 77:2459
Schmitt V, Marques CM, Lequeux F (1995) Phys Rev E 52:4009
Vermant J, Raynaud L, Mewis J, Ernst B, Fuller GG (1999) J Coll Int Sci 211:221
Weissenberg K (1947) Nature 159:310